Light-activated DNA binding in a designed allosteric protein

Devin Strickland, Keith Moffat, and Tobin R. Sosnick*

Department of Biochemistry and Molecular Biology and Institute for Biophysical Dynamics, University of Chicago, 929 East 57th Street, Chicago, IL 60637

Edited by David Baker, University of Washington, Seattle, WA, and approved May 12, 2008 (received for review October 9, 2007)

An understanding of how allostery, the conformational coupling of distant functional sites, arises in highly evolvable systems is of considerable interest in areas ranging from cell biology to protein design and signaling networks. We reasoned that the rigidity and defined geometry of an α-helical domain linker would make it effective as a conduit for allosteric signals. To test this idea, we rationally designed 12 fusions between the naturally photoactive LOV2 domain from *Avena sativa* phototropin 1 and the *Escherichia coli trp* repressor. When illuminated, one of the fusions selectively binds operator DNA and protects it from nuclease digestion. The ready success of our rational design strategy suggests that the helical ''allosteric lever arm'' is a general scheme for coupling the function of two proteins.

allostery | LOV domain | protein design | *trp* repressor | alpha helix

A substantial test of our understanding of protein structure is the design of new molecules with controllable functions, including the rewiring of protein-mediated signaling networks. The modular nature of proteins makes such engineering straightforward in principle. However, the mechanisms by which the components can be allosterically connected are not fully within our control. In one prevalent model, allostery results from intramolecular binding between discrete domains that are linked by regions of undefined structure (1). Although this model has considerable appeal and explanatory power, the discovery of additional mechanisms that are compatible with modular architectures would increase our understanding of signal transduction and facilitate protein-design efforts (2).

New functional architectures evolve through the shuffling of modular domains by genomic insertion and deletion (indel) (3, 4). In one type of indel, domain insertion, two covalent connections between the domains constrain their relative orientation. Allostery in these chimeras is probably related to structural changes at the junctions (5, 6). Protein designers have used domain insertion to create allosteric switches with mechanisms ranging from subtle conformational changes to mutually exclusive folding (7–9). A conceptually similar approach has been used successfully to engineer highly-modular RNA switches (10). The other type of indel, end-to-end fusion, imposes fewer constraints on the relative orientation of the domains, especially if the linker region is unstructured. On the one hand, few structural constraints may favor easy evolvability; on the other hand, possible mechanisms of allosteric coupling may be excluded.

Allostery, once regarded as an evolutionarily refined property occurring only in oligomeric proteins, is now understood to be quite common and readily exploited by evolution or by design (11–14). Reinforcing this idea, especially with respect to modular signaling proteins, is the observation that the deactivation of a protein can be accomplished by any perturbation that disrupts the active site (15). Allosteric effectors may be small molecules, peptides, or other proteins that bind to a site distant from the active site. Alternatively, allostery may be associated with inter- and intramolecular binding interactions that cause either steric occlusion of the active site or domain rearrangements acting on short linkers so that strain is introduced into the structure (1, 16, 17). Nevertheless, designers have created systems that do not fit easily with this framework. Guntas and Ostermeier (18) recovered from a library an allosteric end-to-end fusion of β-lactamase and maltose-binding protein, domains that do not naturally associate. It remains unclear whether allostery in end-to-end fusions can be associated with structural changes in the linker regions in the absence of conserved interdomain interactions.

Discussion

Design Strategy. We reasoned that an allosteric switch could be created by joining two domains so that they share a continuous helix (Fig. 1*A*). By itself, this type of fusion can result in a single well folded protein, as shown by Bai, and coworkers (17, 19). To create an allosteric switch with a bistable energy surface having two alternative wells, we built the fusions to have a steric domain–domain overlap if the shared helix assumes its normal position in both domains. Because residues in regular helices are confined to a narrow region of the Ramachandran map of backbone dihedral angles, bending of an α-helix is energetically unfavorable (20). As a consequence, the shared helix acts as a rigid lever arm, and the overlap is most readily relieved by the disruption of contacts between the shared helix and one domain or the other.

Because these helical contacts are integral to the structure of the domains, their disruption will cause a global shift in the conformational ensemble (11, 21, 22). Conversely, a perturbation such as ligand binding or photoexcitation, which changes the conformational ensemble of the protein, will also change the stability of the helix–domain contacts. This change shifts the relative affinity of the shared helix for each of the two domains, thereby allowing a signal sensed by one domain to be allosterically propagated to the other domain. With this concept in mind, we designed a light-controlled DNA-binding protein.

As a light-sensitive input module, we chose the photoactive LOV2 domain of *Avena sativa* phototropin1 (AsLOV2) (Fig. 1*B*). LOV domains, widely distributed in modular signaling architectures, contain a cofactor-binding PAS domain flanked by amino- and/or carboxyl-terminal helices (23–26). In AsLOV2, absorption of a photon leads to the formation of a covalent adduct between the flavin mononucleotide (FMN) cofactor and a conserved cysteine residue (27). This adduct decays spontaneously to the ground state in tens of seconds. Adduct formation is accompanied by the displacement and unfolding of the 20-residue carboxyl-terminal Jα-helix from the LOV domain, an event that likely mediates signal propagation in its biological context (28, 29).

As an output module, we chose the bacterial transcription factor *trp* repressor (TrpR) (Fig. 1*C*). TrpR, with its L-tryptophan cofactor, binds its operator DNA as a homodimer (30). Mutations

Author contributions: D.S., K.M., and T.R.S. designed research; D.S. performed research; D.S., K.M., and T.R.S. analyzed data; and D.S., K.M., and T.R.S. wrote the paper.

A patent application relating to this work has been filed for which D.S., K.M., and T.R.S. are coinventors.

This article is a PNAS Direct Submission.

*To whom correspondence should be addressed at: Department of Biochemistry and Molecular Biology, University of Chicago, 929 E. 57th Street, GCIS W101C, Chicago, IL 60637. E-mail: trsosnic@uchicago.edu.

This article contains supporting information online at www.pnas.org/cgi/content/full/0709610105/DCSupplemental.

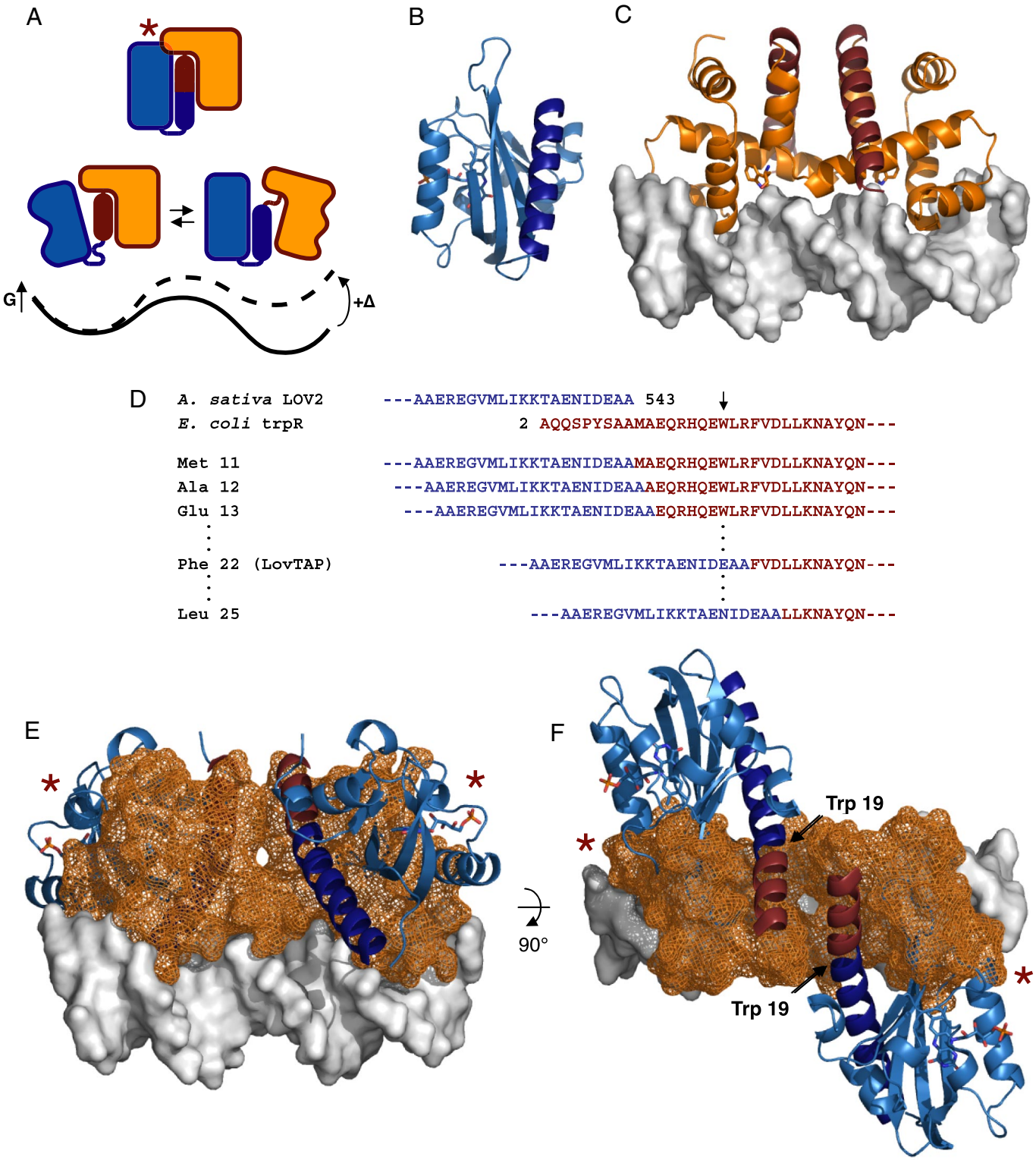

Fig. 1. Design of an allosteric, light-activated repressor. (*A*) Conceptual model of an allosteric lever arm. Joining two domains across terminal α-helices creates a bistable system in which steric overlap (red star) is relieved by the disruption of contacts between the shared helix and one or the other of the domains. A perturbation (Δ) such as ligand binding or photoexcitation alters the energy surface of the system (black line) to favor a new conformational ensemble (dashed line) with different functional properties. (*B*) The LOV2 domain (46) of *A. sativa* phototropin 1 (PDB ID code 2VOU, light blue ribbon) showing the carboxyl-terminal Jα-helix (dark blue ribbon). (*C*) An *E. coli* TrpR dimer (PDB ID code 1TRR, orange ribbon) bound to operator DNA (gray surface). The amino terminus of the protein is an α-helix (red). (*D*) Sequence of the Jα-helix of LOV2 through Ala 543 and of the amino terminus of TrpR beginning with Ala 2. The sequences are shown in the same colors as the models in *A* and *B*. Trp 19 of TrpR is indicated with an arrow. For this study, we created a series of constructs in which the LOV2 domain, intact through Ala 543, is fused to successive truncations of the amino-terminal helix of TrpR beginning with Met 11. (*E* and *F*) Dark-state model of LovTAP (colors same as in *A* and *B*; TrpR domain shown in orange mesh). Red stars denote regions of steric overlap. Models have been represented by using PyMOL (www.pymol.org).

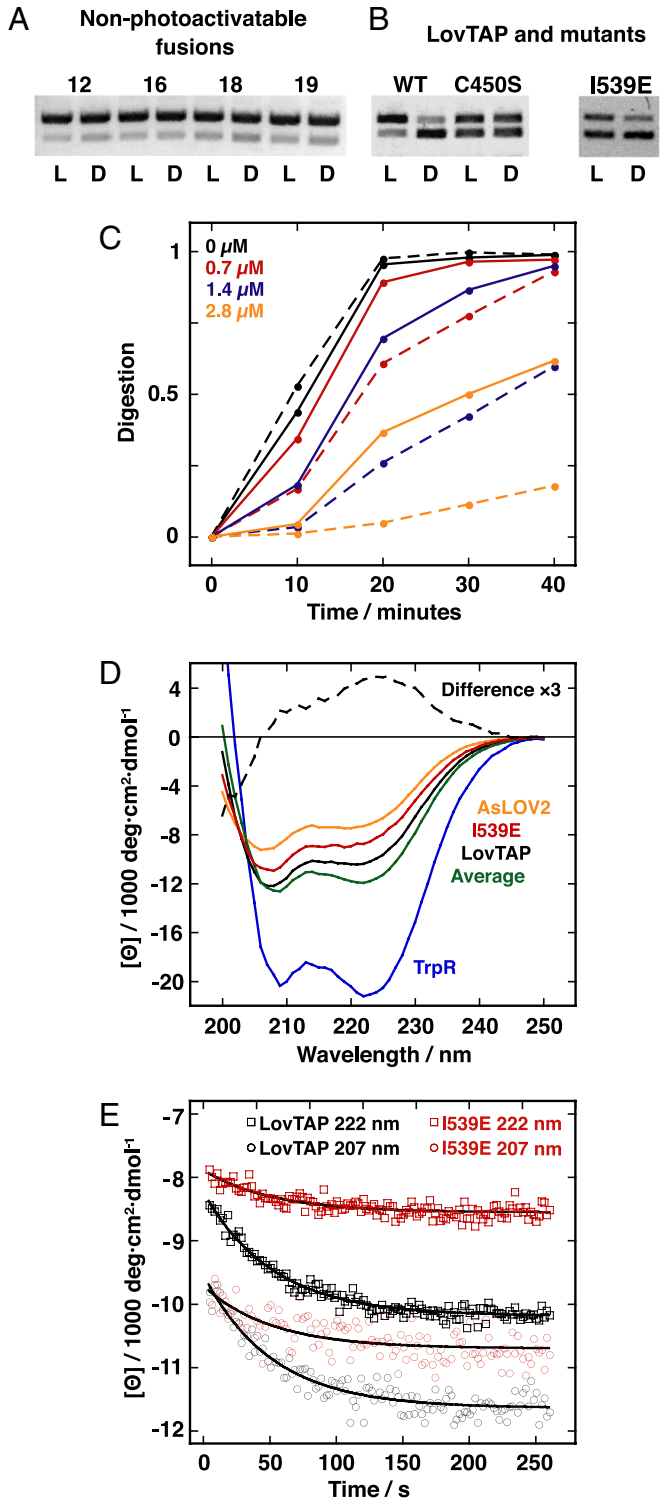

Fig. 2. Light-induced protection of operator DNA by LovTAP and associated structural changes. (*A*) DNA protection in the light (L) and dark (D) at 50 nM protein monomer. The examples shown are representative of all constructs except LovTAP. (*B*) DNA protection in the light and dark at 130 nM LovTAP monomer. (*C*) Light and dark activity of LovTAP. Solid lines, dark reactions; dashed lines, illuminated reactions. Digestion is the intensity ratio of the sum of product bands to the sum of the product bands plus the reactant band. The colored concentrations indicate the LovTAP monomer concentration in the reaction mixture. (*D*) Dark-state, far-UV CD spectra. LovTAP and the I539E mutant are shown, as are LOV2 and TrpR. The green line (Average) is the residue-weighted average of LOV2 and TrpR. The dashed line (Difference ×3) is the difference of the LovTAP spectrum and the residue-weighted average spectrum multiplied by three. (*E*) Kinetic recovery of CD from steady-state photoexcitation for LovTAP and the I539E mutant. Exponential fits are shown as solid lines.

throughout the protein, including those in the 21-residue amino-terminal helix, affect cofactor and operator binding, suggesting the presence of many allosterically sensitive sites (31–34). Isolated TrpR domains occur widely in bacteria but are not known to participate in modular architectures.

Isolation of a Light-Sensitive DNA-Binding Protein. We ligated AsLOV2 (residues 404–543) via its carboxyl-terminal Jα-helix to a succession of 13 amino-terminal truncations of TrpR (residues 11–108) (Fig. 1*D*). We chose residue 11 as the amino-terminal boundary of TrpR because this amino acid is the first helical residue in the crystal structure (35). Upon purification, we found that FMN binding and reversible photobleaching are preserved in all constructs (27). Furthermore, using a plasmid-based RsaI protection assay, we found that all constructs specifically protect cognate DNA against nuclease digestion under ambient light, although they do so to differing degrees depending on the truncation of the TrpR domain (36) [supporting information (SI) Fig. S1].

One construct, which we refer to as the LOV- and tryptophan-activated protein (LovTAP), preferentially protects cognate DNA when illuminated (Fig. 2 *A*–*C*). This construct joins the carboxyl terminus of the Jα-helix of the LOV domain to the middle of the amino-terminal helix of TrpR at Phe 22 (Fig. 1*D*). At saturating photoexcitation (20 mW·cm^{-2} irradiance at 470 nm) and micromolar LovTAP concentration, the apparent rate of RsaI digestion of cognate DNA is decreased compared with the rate in the dark. DNA binding is specific for the *trp* operator and requires free L-tryptophan (data not shown), suggesting that LovTAP binds DNA in a manner that is characteristic of the TrpR domain. Mutation of the photoactive cysteine of the LOV domain to serine prevents the normal photocycle and abolishes the light sensitivity of DNA protection. Therefore, the activation of LovTAP originates with photochemical events involving the FMN cofactor (27).

To quantify the effectiveness of the LovTAP design, we determined its binding affinity for operator DNA in the dark and lit states. In a modified RsaI protection assay with a DNA fragment having only one cleavage site, the observed cleavage rate was the intrinsic rate multiplied by the fractional occupancy of LovTAP at the cleavage site (Table 1 and Fig. S2). For nanomolar LovTAP concentrations, the observed cleavage rates indicated average DNA-binding affinities of 142 ± 61 nM and 788 ± 94 nM in the lit and dark states, respectively. Therefore, photoexcitation of LovTAP increases the K_d of DNA binding by a factor of 5.6 ± 2.5.

Structure and Mechanism of LovTAP. We tested whether the shared helix is implicated in the allosteric behavior of LovTAP by measuring the helical content in the dark and lit states using far-UV CD spectroscopy. The dark-state CD spectrum of LovTAP is close to the residue-weighted average of the dark-state AsLOV2 spectrum and the TrpR spectrum (Fig. 2*D*) (32, 37). The difference of these two spectra indicates that some of the α-helix present in AsLOV2 or TrpR has been lost in the fusion and replaced with random coil (Fig. 2*D*). This result is expected because 11 helical TrpR residues were truncated in making the construct, and at least some of the remaining helical residues are predicted to be unfolded in the dark state. Mutating residues Ile 532, Ala 536, or Ile 539 of AsLOV2, which lie on the Jα-helix and contact the β-sheet, to a charged glutamic acid leads to a pseudolit-state structure (28). In the dark state, these mutants have a less negative CD signal at 222 and 207 nm than LovTAP, consistent with the mutations partially unfolding the shared helix (Fig. 2*D*, I532E and A536E not shown). Under saturating photoexcitation, all three variants have similar CD signals

Table 1. Dark- and lit-state DNA binding

[LovTAP], mM	k_0^{dark}, min^{-1}	k_0^{lit}, min^{-1}	k_{obs}^{dark}, min^{-1}	k_{obs}^{lit}, min^{-1}	K_d^{dark}, nM	K_d^{lit}, nM	K_d^{dark}/K_d^{lit}
285	0.127 ± 0.004	0.139 ± 0.007	0.093 ± 0.004	0.044 ± 0.002	788 ± 61	132 ± 29	5.9 ± 1.4
440	0.083 ± 0.005	0.091 ± 0.004	0.059 ± 0.005	0.018 ± 0.002	1074 ± 148	107 ± 79	10 ± 7.6
690	0.13 ± 0.02	0.12 ± 0.02	0.052 ± 0.005	0.025 ± 0.0001	502 ± 232	186 ± 163	2.7 ± 2.7
Average	NA	NA	NA	NA	788 ± 94	142 ± 61	5.6 ± 2.5

k_0 is the intrinsic rate of digestion of DNA by RsaI. k_{obs} is the rate of digestion of DNA by RsaI in the presence of LovTAP. K_d is the dissociation constant of the binding reaction of LovTAP to cognate DNA. NA, not applicable.

at 222 nm (−8,000 deg·cm²·dmol⁻¹) and at 207 nm (−9,500 deg·cm²·dmol⁻¹), suggesting similar structures (Fig. 2*E*). In full-length phototropin 1, the I532E, A536E, and I539E mutations in the LOV2 domain decouple kinase activity from photoexcitation (28). Similarly, in LovTAP, these mutations decouple DNA protection from photoexcitation, implicating the Jα-helix in the mechanism of allosteric signal propagation (Fig. 2*B*, I532E and A536E not shown).

We built a dark-state model of LovTAP by assuming that the carboxyl-terminal Jα-helix of LOV2 and the amino-terminal helix of TrpR form a structurally continuous, shared helix across the point of ligation (Fig. 1 *E* and *F*). Steric overlaps occur between the LOV domains and the TrpR domain, suggesting that contacts between the shared helix and one or both of the parent domains must be disrupted to relieve the strain. Given that the Jα-helix readily dissociates from the core of AsLOV2, whereas wild-type TrpR is a tight, intertwined dimer (34), the shared helix should strongly associate with the TrpR domain in the context of LovTAP. However, this construct includes a destabilizing substitution of TrpR residue Trp 19 with glutamic acid. Trp 19, the first conserved residue in bacterial TrpR domains and the first residue in the primary sequence of *Escherichia coli* TrpR to participate in the hydrophobic core, pins the amino-terminal helical arm to the body of the protein. TrpR, alone and in LOV2–TrpR constructs, tolerates changes at this highly conserved position but always with a diminution of DNA-binding activity (31) (Fig. S1). Upon the destabilizing W19E substitution in LovTAP, a few residues of the shared helix presumably dissociate from the TrpR domain and dock against the LOV domain. In this configuration, the steric overlap is relieved, but the TrpR domain has decreased DNA-binding affinity, a weaker monomer–dimer equilibrium, or both (38) (Fig. S3 *A* and *B*). Upon photoinduced displacement from the LOV domain, the residues reassociate with the TrpR domain, thus restoring DNA-binding affinity (Fig. 3).

We further investigated the overall size and shape of the dark-state structure of LovTAP using synchrotron-based small-angle x-ray scattering (SAXS). At 4, 8, and 16 μM LovTAP, the radius of gyration (R_g) is 29–30 Å (Fig. 4*A* and Table 2). The experimental $P(r)$ pair-distribution function compares well with a distribution calculated from our model (39, 40) (Fig. 4*B*). The molecular envelope reconstructed from the data also agrees well with the model (41) (Fig. 4*C*). The reconstruction is slightly longer than the model, with excess density peripheral to the LOV domains. Because our model is built with a continuous shared helix and steric overlap between the domains, it is presumably overly compact compared with the true structure. However, in the dark state, the LOV domains clearly do not occlude the DNA-binding surface of the TrpR domain, reinforcing our proposed mechanism in which inactivation is accomplished by deformation of the TrpR domain.

Implications for Allosteric Signaling Proteins. Given the simplicity and ready success of the shared helix design strategy, we searched for naturally occurring examples. The amino terminus of Cbl (Cbl-N) includes an SH2 domain, an EF-hand domain, and a four-helix bundle domain in a compact, integrated structure (42). Mutation of calcium ligands of the EF-hand reduces phosphopeptide binding, indicating allosteric coupling between the SH2 and EF-hand domains. A nonconserved, shared helix connects the SH2 domain and the EF hand domain, packing against both. Phosphopeptide binding rotates the SH2 domain toward the four-helix bundle domain, twisting the shared helix and subtly distorting the EF hand domain.

Most natural photosensory proteins have a highly conjugated chromophore and respond to the absorption of a photon with either a *cis–trans* isomerization of a double bond or, in the case of LOV domains, the formation of a covalent adduct between the protein and chromophore (43). This local change in geometry is propagated to the rest of the protein domain, thus altering its conformational ensemble. Many LOV domains contain an amino- or carboxyl-terminal helix, which docks against the core β-sheet opposite the bound chromophore and responds to photoexcitation with a conformational change (26). Our results suggest that with appropriate consideration of the linker structure, it may be quite straightforward to design photoactive switches in which LOV domains are coupled to a large number of diverse output domains.

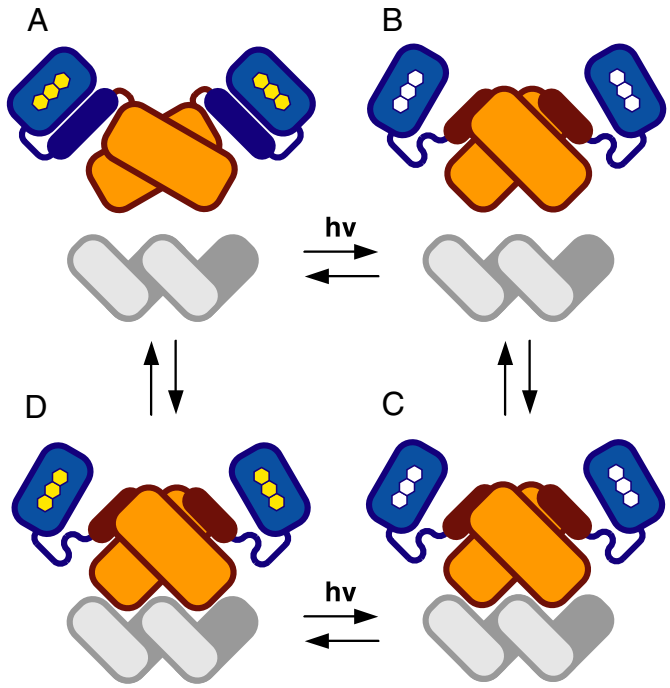

Fig. 3. Proposed mechanism for LovTAP function. The LOV domain is shown in light blue, the TrpR domain in orange, and the operator DNA in gray. The shared helix is shown in dark blue when contacting the LOV domain and in red when contacting the TrpR domain. The three-ring FMN chromophore is shown in yellow in the ground state and white when photoexcited. (*A*) In the dark DNA-dissociated state, the shared helix contacts the LOV domain, populating an inactive conformation of the TrpR domain. (*B*) Photoexcitation disrupts contacts between the shared helix and the LOV domain, populating an active conformation of the TrpR domain. (*C*) LovTAP binds DNA. (*D*) The LOV domains return to the dark state. LovTAP dissociates from the DNA, contacts between the shared helix and the LOV domain are restored, and the system returns to the initial state.

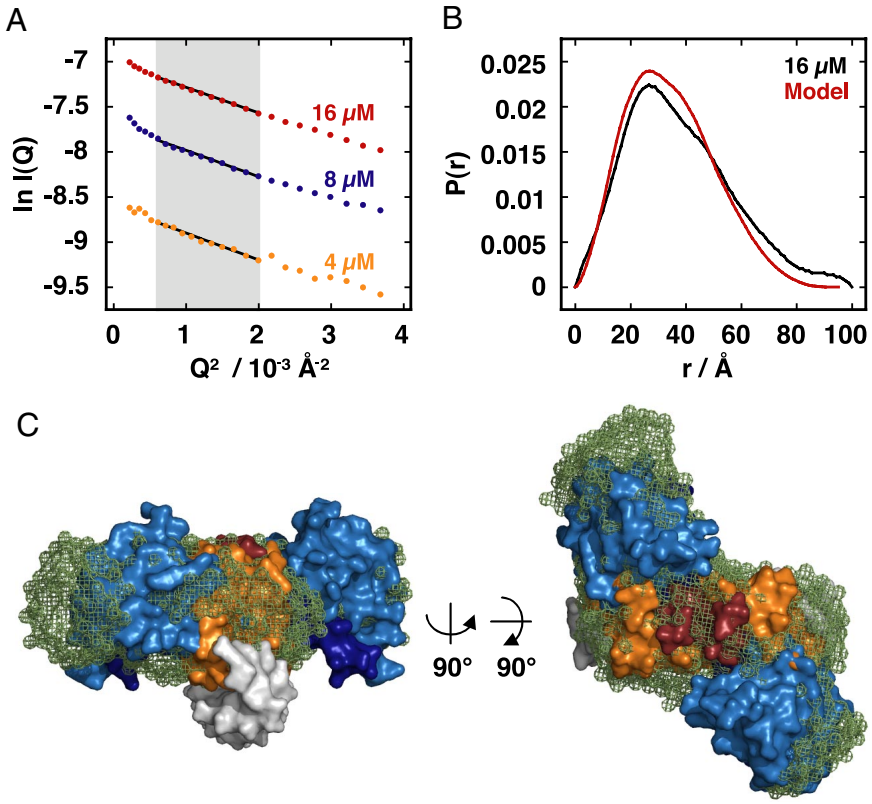

Fig. 4. SAXS analysis of LovTAP dark-state structure. (*A*) Guinier plots. The shaded area indicates the range of fitting for R_g analysis ($R_g \cdot Q \leq 1.3$). (*B*) P(r) pair-distribution function plots. The black line is calculated from the [LovTAP] = 16 μM data. The red line is calculated from the LovTAP dark-state model, including an unstructured amino-terminal calmodulin-binding peptide (R_g = 26.9 Å). (*C*) Model of LovTAP compared with *ab initio* dark-state reconstruction from the SAXS data. The reconstruction, shown as green mesh, is manually aligned with the model of LovTAP, shown as a surface by using the same colors as in Fig. 1. DNA was not present in the experiment but is shown here in gray. The calmodulin-binding peptide is not shown.

We propose that LovTAP samples two conformations, an activated conformation in which the shared helix is associated with the TrpR domain and an inactivated conformation in which the helix is associated with the LOV domain. Because photoactivation decreases the affinity of the LOV domain for the shared helix, it shifts the conformational ensemble toward the active conformation. Conversely, dark-state recovery increases the affinity of the LOV domain for the helix and shifts the ensemble back toward the inactivated conformation. This population shift is the source of the 6-fold change in DNA-binding affinity. Accordingly, the maximal change in DNA-binding affinity is limited by the LOV–helix affinity in the dark state. For the isolated AsLOV2 domain, the dark state K_a = 61.5 (X. Yao, M. K. Rosen, and K. H. Gardner, personal communication). Therefore, the maximum switching provided by the LOV domain available should be 65-fold (or 65^2-fold, assuming both shared helices in the dimer must independently associate with the TrpR domain for full activity). It will be interesting to explore whether this limit can be approached or exceeded by increasing the affinity of the LOV domain for the shared helix.

Table 2. Small-angle scattering results

[LovTAP]	R_g (Guinier)*	R_g [P(r)]	I_o/conc†
4 μM (0.13 mg/ml)	29.9 ± 0.6 Å	29.2 ± 0.5 Å	0.8 ± 0.0
8 μM (0.25 mg/ml)	29.5 ± 0.2 Å	29.8 ± 0.2 Å	1.0 ± 0.0
16 μM (0.5 mg/ml)	29.2 ± 0.1 Å	29.8 ± 0.1 Å	1.0 ± 0.0

*R_g is calculated from both the Guinier analysis of the scattering intensity and the second moment of the P(r) pair-distribution function.

†The zero angle scattering, I_o, divided by the protein concentration is proportional to the molecular weight of the molecule and is normalized to the value at [LovTAP] = 16 μM.

Conclusions

Our successful design of an allosteric lever arm and a bistable energy surface, along with the observation of a natural analogue, suggest the existence of a general but largely unrecognized mode of connecting modular domains into a functionally integrated whole. The α-helical structure of the linker distinguishes this mode from others in which allostery results from intramolecular binding between domains connected by linkers of undefined structure (1). Because a regular helix resists bending and twisting, it can function as an allosteric lever arm to transmit forces created by interdomain contacts to generate bistable systems. Given the predominance of end-to-end fusion in modular architectures, we anticipate that more examples of shared helices will be found in naturally occurring signaling proteins.

Materials and Methods

Cloning, Expression, and Purification. The DNA fragment encoding *E. coli* TrpR was obtained by colony PCR. A clone of *A. sativa* phot1 LOV2 was generously provided by Kevin Gardner (University of Texas Southwestern Medical Center, Dallas). The fusion proteins were created from these templates by using overlap extension PCR and subcloned into the expression vector pCal-n (Stratagene). The fusion proteins were expressed in *E. coli* and purified. See *SI Materials and Methods* for details.

Illumination. Blue AlGaInP LEDs (theledlight.com) were used for illumination. The radiant power delivered to the samples was estimated by using a hand-held power meter (New Focus). Irradiance was calculated by using 0.12 cm^2 as the cross-sectional area of the reaction tube. See *SI Materials and Methods* for details.

RsaI Protection Assay (36). A plasmid containing two natural RsaI sites and one site buried in a *trp* operator was digested with RsaI. TrpR activity protects the 1,890-bp fragment from digestion by RsaI to the 1,410- and 480-bp products. A 676-bp internal control results from digestion at unprotected sites. For simplicity, only the 1,890- and 1,410-bp fragments are shown in the figures. Digestion was determined as the ratio of the intensity of the product bands (1,410 and 480 bp) to that of the product bands plus the reactant band (1,890 bp). See *SI Materials and Methods* for details.

Modified RsaI Protection Assay. We modified the above assay to simplify the reaction scheme so that the data are interpretable by using a single exponential model. Other than the substitution of the DNA substrate, the assay was performed essentially as described above. For all fits, the amplitude was constrained to unity, and only the rate was allowed to vary. K_d in the lit and dark states was calculated according to $K_d = L/(R - 1)$, where L is the concentration of LovTAP, and R is the ratio of the intrinsic rate of RsaI digestion (k_0) and the rate in the presence of LovTAP (k_{obs}). See *SI Materials and Methods* for details.

CD Spectroscopy. CD measurements were performed at 1–7 μM protein in 150 mM KPO_4 (pH 7.0), 1 mM EDTA, at 25°C, 0.1-cm path-length cuvette. For kinetic experiments, illumination was from a single blue LED connected to an external switch. The sample was illuminated for 30 s to saturated photoexcitation, and then the LED was switched off and data recorded for 250 s. CD at 222 and 207 nm were recorded in triplicate, averaged, and fit to a single exponential function by using IGOR Pro (WaveMetrics). See *SI Materials and Methods* for details.

Structural Modeling. Atomic coordinates of *E. coli* TrpR (PDB ID code 1TRR) and *A. sativa* phot1 LOV2 (PDB ID code 2VOU) were analyzed in DeepView (http://www.expasy.org/spdbv/) (44). Structural models were built by aligning the Cα atoms of several residues at the end of the LOV2 Jα-helix with the Cα atoms of the same number of residues on the amino-terminal helix of TrpR, immediately preceding the intended junction. To illustrate the degree of steric overlap accompanying a continuous shared helix, no further adjustments to the structure were made.

SAXS. All SAXS data were collected at the BioCAT beamline at the Advanced Photon Source (Argonne National Laboratory, Argonne, IL). I(Q) data were converted to P(r) data by using GNOM (http:www.embl-hamburg.de/ExternalInfo/Research/Sax/gnom.html) (39). Experimental P(r) data were compared with the distribution calculated (40) from our dark-state model. *Ab initio* reconstructions were generated by using DAMMIN (http://www.embl-hamburg.de/ExternalInfo/Research/Sax/dammin.html) (41) and averaged by using DAMAVER (http://www.embl-hamburg.de/ExternalInfo/Research/Sax/damaver.html) (45). See *SI Materials and Methods* for details.

ACKNOWLEDGMENTS. We thank T. Pan, S. Crosson, P. Rice, S. Koide, P. Nash, R. Keenan, B. Liu, A. Halavaty, J. Kennis, P. Cluzel, W. Lim, K. Gardner, J. Carey, and members of the T.R.S. and K.M. laboratories for helpful discussions and L. Guo and N. Baird for assistance with the SAXS experiments. This work was supported by National Institutes of Health research grants (to K.M. and T.R.S.) and training grants. Use of the Advanced Photon Source was supported by the U.S. Department of Energy, Basic Energy Sciences, Office of Science. BioCAT is a National Institutes of Health-supported research center.

1. Bhattacharyya RP, Remenyi A, Yeh BJ, Lim WA (2006) Domains, motifs, and scaffolds: The role of modular interactions in the evolution and wiring of cell signaling circuits. *Annu Rev Biochem* 75:655–680.
2. Pawson T, Linding R (2005) Synthetic modular systems—Reverse engineering of signal transduction. *FEBS Lett* 579:1808–1814.
3. Pawson T, Nash P (2003) Assembly of cell regulatory systems through protein interaction domains. *Science* 300:445–452.
4. Ponting CP, Russell RR (2002) The natural history of protein domains. *Annu Rev Biophys Biomol Struct* 31:45–71.
5. Ostermeier M (2005) Engineering allosteric protein switches by domain insertion. *Protein Eng Des Sel* 18:359–364.
6. Russell RB (1994) Domain insertion. *Protein Eng* 7:1407–1410.
7. Baird GS, Zacharias DA, Tsien RY (1999) Circular permutation and receptor insertion within green fluorescent proteins. *Proc Natl Acad Sci USA* 96:11241–11246.
8. Guntas G, Mansell TJ, Kim JR, Ostermeier M (2005) Directed evolution of protein switches and their application to the creation of ligand-binding proteins. *Proc Natl Acad Sci USA* 102:11224–11229.
9. Radley TL, Markowska AI, Bettinger BT, Ha JH, Loh SN (2003) Allosteric switching by mutually exclusive folding of protein domains. *J Mol Biol* 332:529–536.
10. Win MN, Smolke CD (2007) A modular and extensible RNA-based gene-regulatory platform for engineering cellular function. *Proc Natl Acad Sci USA* 104:14283–14288.
11. Gunasekaran K, Ma B, Nussinov R (2004) Is allostery an intrinsic property of all dynamic proteins? *Proteins* 57:433–443.
12. Freire E (1999) The propagation of binding interactions to remote sites in proteins: Analysis of the binding of the monoclonal antibody D1.3 to lysozyme. *Proc Natl Acad Sci USA* 96:10118–10122.
13. Hilser VJ, Thompson EB (2007) Intrinsic disorder as a mechanism to optimize allosteric coupling in proteins. *Proc Natl Acad Sci USA* 104:8311–8315.
14. Volkman BF, Lipson D, Wemmer DE, Kern D (2001) Two-state allosteric behavior in a single-domain signaling protein. *Science* 291:2429–2433.
15. Huse M, Kuriyan J (2002) The conformational plasticity of protein kinases. *Cell* 109:275–282.
16. Dueber JE, Yeh BJ, Chak K, Lim WA (2003) Reprogramming control of an allosteric signaling switch through modular recombination. *Science* 301:1904–1908.
17. Sallee NA, Yeh BJ, Lim WA (2007) Engineering modular protein interaction switches by sequence overlap. *J Am Chem Soc* 129:4606–4611.
18. Guntas G, Ostermeier M (2004) Creation of an allosteric enzyme by domain insertion. *J Mol Biol* 336:263–273.
19. Zhou Z, Feng H, Zhou H, Zhou Y, Bai Y (2005) Design and folding of a multidomain protein. *Biochemistry* 44:12107–12112.
20. Jha AK, *et al*. (2005) Helix, sheet, and polyproline II frequencies and strong nearest neighbor effects in a restricted coil library. *Biochemistry* 44:9691–9702.
21. Luque I, Freire E (2000) Structural stability of binding sites: Consequences for binding affinity and allosteric effects. *Proteins Suppl* 4:63–71.
22. Whitten ST, Garcia-Moreno EB, Hilser VJ (2005) Local conformational fluctuations can modulate the coupling between proton binding and global structural transitions in proteins. *Proc Natl Acad Sci USA* 102:4282–4287.
23. Huala E, *et al*. (1997) *Arabidopsis* NPH1: A protein kinase with a putative redox-sensing domain. *Science* 278:2120–2123.
24. Key J, Hefti M, Purcell EB, Moffat K (2007) Structure of the redox sensor domain of *Azotobacter vinelandii* NifL at atomic resolution: Signaling, dimerization, and mechanism. *Biochemistry* 46:3614–3623.
25. Crosson S, Rajagopal S, Moffat K (2003) The LOV domain family: Photoresponsive signaling modules coupled to diverse output domains. *Biochemistry* 42:2–10.
26. Zoltowski BD, *et al*. (2007) Conformational switching in the fungal light sensor Vivid. *Science* 316:1054–1057.
27. Swartz TE, *et al*. (2001) The photocycle of a flavin-binding domain of the blue light photoreceptor phototropin. *J Biol Chem* 276:36493–36500.
28. Harper SM, Christie JM, Gardner KH (2004) Disruption of the LOV-Jalpha helix interaction activates phototropin kinase activity. *Biochemistry* 43:16184–16192.
29. Harper SM, Neil LC, Gardner KH (2003) Structural basis of a phototropin light switch. *Science* 301:1541–1544.
30. Gunsalus RP, Yanofsky C (1980) Nucleotide sequence and expression of *Escherichia coli* trpR, the structural gene for the trp aporepressor. *Proc Natl Acad Sci USA* 77:7117–7121.
31. Chapman D, Hochstrasser R, Millar D, Youderian P (1995) Engineering proteins without primary sequence tryptophan residues: Mutant trp repressors with aliphatic substitutions for tryptophan side chains. *Gene* 163:1–11.
32. Jin L, Fukayama JW, Pelczer I, Carey J (1999) Long-range effects on dynamics in a temperature-sensitive mutant of trp repressor. *J Mol Biol* 285:361–378.
33. Mackintosh SG, McDermott PF, Hurlburt BK (1998) Mutational analysis of the NH2-terminal arms of the trp repressor indicates a multifunctional domain. *Mol Microbiol* 27:1119–1127.
34. Reedstrom RJ, *et al*. (1996) Characterization of charge change super-repressor mutants of trp repressor: Effects on oligomerization conformation, ligation and stability. *J Mol Biol* 264:32–45.
35. Lawson CL, Carey J (1993) Tandem binding in crystals of a trp repressor/operator half-site complex. *Nature* 366:178–182.
36. Joachimiak A, Kelley RL, Gunsalus RP, Yanofsky C, Sigler PB (1983) Purification and characterization of trp aporepressor. *Proc Natl Acad Sci USA* 80:668–672.
37. Corchnoy SB, *et al*. (2003) Intramolecular proton transfers and structural changes during the photocycle of the LOV2 domain of phototropin 1. *J Biol Chem* 278:724–731.
38. Shao X, Hensley P, Matthews CR (1997) Construction and characterization of monomeric tryptophan repressor: A model for an early intermediate in the folding of a dimeric protein. *Biochemistry* 36:9941–9949.
39. Svergun DI (1992) Determination of the regularization parameter in indirect-transform methods using perceptual criteria. *J Appl Cryst* 25:495–503.
40. Thiyagarajan P, Henderson SJ, Joachimiak A (1996) Solution structures of GroEL and its complex with rhodanese from small-angle neutron scattering. *Structure (London)* 4:79–88.
41. Svergun DI (1999) Restoring low resolution structure of biological macromolecules from solution scattering using simulated annealing. *Biophys J* 76:2879–2886.
42. Meng W, Sawasdikosol S, Burakoff SJ, Eck MJ (1999) Structure of the amino-terminal domain of Cbl complexed to its binding site on ZAP-70 kinase. *Nature* 398:84–90.
43. Hellingwerf KJ (2002) The molecular basis of sensing and responding to light in microorganisms. *Ant V Leeuwenhoek* 81:51–59.
44. Guex N, Peitsch MC (1997) SWISS-MODEL and the Swiss-PdbViewer: An environment for comparative protein modeling. *Electrophoresis* 18:2714–2723.
45. Volkov VV, Svergun DI (2003) Uniqueness of *ab initio* shape determination in small-angle scattering. *J Appl Cryst* 36:860–864.
46. Halavaty AS, Moffat K (2007) N- and C-terminal flanking regions modulate light-induced signal transduction in the LOV2 domain of the blue light sensor phototropin 1 from *Avena sativa*. *Biochemistry* 46:14001–14009.